Asia-Pac. J. Atmos. Sci., 54(s), 361-370, 2018
DOI:10.1007/s13143-018-0013-3
pISSN 1976-7633 / eISSN 1976-7951

Impacts of Shallow Convection Processes on a Simulated Boreal Summer Climatology in a Global Atmospheric Model

Song-You Hong[1] and Jihyeon Jang[2]

[1]*Korea Institute of Atmospheric Prediction Systems (KIAPS), Seoul, Korea*
[2]*National Center for Atmospheric Research/Mesoscale Microscale Meteorology Division, Boulder, Colorado, USA*

(Manuscript received 04 July 2017; accepted 27 January 2018)

Abstract: This study investigates the impacts of shallow convection schemes on a simulated seasonal climatology in the Global and Regional Integrated Model system (GRIMs). The eddy-diffusivity scheme of Tiedtke (TDK) is evaluated, focusing on the dependency upon deep convection schemes. Drying and warming near the top of the planetary boundary layer (PBL) and opposing effects above are observed. The height of PBL is reduced due to the increase of thermal stability near the PBL top. The weakened PBL turbulence is partly compensated with the increased downward solar radiation due to the reduction of low clouds. These effects are pronounced over the oceans, which leads to the modulation of tropical precipitation. It is found that the original TDK scheme shows similar behavior regardless of the choice of deep convection schemes. A revised TDK scheme that explicitly couples the PBL and shallow convection processes is proposed and evaluated. The proposed scheme generally improves the simulated climatology over the results with the original TDK scheme, along with further improvement in the case of the revised deep convection scheme. Our results indicate that the role of the shallow convection scheme needs to be carefully examined to improve the performance of atmospheric models, with a focus on modulated PBL and deep convection processes.

Key words: Shallow convection, deep convection, seasonal forecasts, general circulation model

1. Introduction

Shallow trade wind cumulus is regarded as one of the dominant types of clouds in tropics (Johnson et al., 1999) and a considerable amount of stratocumulus in subtropics is sustained by the shallow cumulus convection (Norris, 1999). The physical processes related to the shallow cumulus play an important role in a general circulation model. By vertical transport of heat and moisture from the boundary layer into the free atmosphere, shallow convection redistributes temperature and moisture. This phenomenon causes a direct effect in the distribution of low clouds, which affects global radiation budgets (Hartmannn et al., 1992; Klein and Hartmann, 1993; Ma et al., 1996; Gordon et al., 2000). Recently, mechanisms affecting the transition from shallow to deep convection have been studied (Wu et al., 2009; Zhang and Klein, 2010).

In atmospheric models, the shallow convection algorithm is regarded as non-precipitating cumulus convection over the precipitating convection due to the cumulus parameterization scheme (Stensrud, 2007). Due to its importance, shallow convection scheme has been incorporated into most of global models for climate simulations or weather forecasts. Historically, precipitating deep convection processes have mainly been focused in modeling community since it directly determines precipitation and associated overturning of temperature and moisture in modeled climate. Meanwhile, studies in shallow convection are relatively rare. Since Tiedtke et al. (1988) examined the impact of shallow cumulus convection on large-scale tropical circulations in the forecast system of the European Centre for Medium-Range Weather Forecasts, subsequent studies using general circulation models (GCMs) investigated the role of non-precipitation convection algorithm for weather and climate forecasts (Slingo et al., 1994; Jakob and Siebesma, 2003; Bretherton and Park, 2009; Han and Pan, 2011; Bogenschutz et al., 2013). Some deep convection schemes include the shallow convection processes (e.g., Betts, 1986). This algorithm can be largely classified by the eddy diffusivity approach (e.g., Tiedtke et al., 1988), and the mass-flux approach (e.g., Bretherton and Park, 2009; Han and Pan, 2011). Meanwhile, Bogenschutz et al. (2013) proposed a unified parameterization of the planetary boundary layer (PBL) and shallow convection that is centered around a trivariate probability density function (PDF) and replaces the conventional PBL, shallow convection, and cloud macrophysics schemes.

This study investigates the impacts of a shallow convection scheme on a simulated seasonal climatology in a global atmospheric model. The eddy-diffusivity scheme based on Tiedtke et al. (1988) is evaluated for a boreal summer climatology. The role of shallow convection in different deep convection schemes is examined in order to understand the impacts of the interaction between the shallow and deep convection processes. A revised eddy-diffusion scheme from the Tiedtke et al. (1988) is proposed and evaluated.

Section 2 describes the model and experimental design, together with the characteristics of two selected convection schemes. Results are discussed in section 3, and a summary is given in the final section.

Corresponding Author: Song-You Hong, Korea Institute of Atmospheric Prediction Systems (KIAPS) 4F, 35 Boramae-ro 5gil, Dongjak-gu, Seoul 07071, Korea.
E-mail: songyou.hong@kiaps.org

2. Model and experimental setup

a. Model

The model used in this study is the Global and Regional Integrated Model system (GRIMs; Hong et al., 2013). The physics package of the model is the GRIMs version 3.1 that includes long- and shortwave radiation, land surface processes, simple hydrology, planetary boundary-layer processes, gravity-wave drag, deep and shallow convection, cloud-radiation interaction, diagnostic large-scale precipitation physics on clouds, and vertical and horizontal diffusions. This model system has been created for use in numerical weather prediction, seasonal simulations, and climate research projects, from global to regional scales. The very initial version of global and regional models is rooted in the National Centers of Environmental Prediction (NCEP) seasonal forecast model (Kanamitsu et al., 2002a) and regional spectral model (Juang and Kanamitsu, 1994; Juang et al., 1997), but with subsequent developments of model physics and dynamics, along with the reconfiguration of code structure. GRIMs is greatly flexible with multi- platforms, with either multithreaded shared memory or message- passing interface (MPI) modes. Refer to Hong et al. (2013) for further details. For the deep convection physics, the Simplified Arakawa-Schubert (SAS) convective parameterization scheme (CPS), developed by Pan and Wu (1995) based on Grell (1993), in NCEP-Department of Energy (NCEP-DOE) Reanalysis II dataset (RA2; Kanamitsu et al., 2002b) and the modified version of the SAS scheme (Han and Pan, 2011) for the new physics package of the NCEP Global Forecast System (GFS) are used. In this study, the former and latter schemes are named the RA2 CPS and GFS CPS, respectively.

b. Description of the Tiedtke shallow convection scheme

The Tiedtke (TDK, hereafter) shallow convection (SCV, hereafter) scheme has been operational in the NCEP GFS until it was replaced by the Han and Pan scheme in July 2010. The TDK scheme represents the effects of shallow convection on temperature and specific humidity by using an eddy diffusivity approach with the prescribed coefficients. When the parcel is lifted between the surface and 700 hPa and the layers are conditionally unstable, the shallow convection scheme starts to calculate the additional vertical mixing of heat and moisture within cloud layer through vertical diffusion equation such as

$$\frac{\partial T}{\partial t} = \frac{1}{\rho}\frac{\partial}{\partial z}\left(\rho K\left[\frac{\partial T}{\partial z}+\Gamma\right]\right) \tag{1}$$

$$\frac{\partial q}{\partial t} = \frac{1}{\rho}\frac{\partial}{\partial z}\left(\rho K\frac{\partial q}{\partial z}\right) \tag{2}$$

and

$$\begin{aligned} K &= 1\ \mathrm{m^2\,s^{-1}} \text{ at the cloud top,} \\ &= 3\ \mathrm{m^2\,s^{-1}} \text{ at a level below the cloud top,} \\ &= 1.5\ \mathrm{m^2\,s^{-1}} \text{ at the cloud bottom,} \\ &= 5\ \mathrm{m^2\,s^{-1}} \text{ otherwise} \end{aligned} \tag{3}$$

where T is temperature, q is specific humidity, K is the eddy diffusivity, Γ is a lapse rate, ρ is density of air, and z is height from the surface. In this scheme, K is specified as in (3), thus the thermodynamic changes around the shallow cumulus depend on the vertical shape of the environmental variables. The cloud bottom is defined as the lifting condensation level (LCL) of an updraft air parcel originating near the surface, and its top is the neutral buoyancy level. The maximum height of clouds is limited to the level of about 3 km from the surface (sigma = 0.7) More details of the TDK scheme are described in Tiedtke et al. (1988).

c. Revisions to the Tiedtke scheme

It is noted that the diffusion coefficient in (3) is empirically determined, although it mimics a parabolic shape. Thus, it is changed as

$$K = RH \times w \times \delta \times \left(1-\frac{z_b+h}{D+h}\right)^2 \tag{4}$$

where RH designates the relative humidity at the PBL top, h. The mixed layer velocity scale at the PBL top, w, and the entrainment depth, δ, are computed in the Yonsei University (YSU) PBL scheme (see the appendix of Hong et al., 2006). w is a function of friction velocity and buoyancy fluxes at the surface layer. z_b is the height from the cloud bottom and D is the cloud depth. h is determined as the neutral buoyancy level by checking the bulk Richardson number between the thermal and the height from the surface, where the thermal is defined as a sum of virtual potential temperature at the surface layer and thermal excess term that is a function of surface fluxes. δ is a function of stability at h. The exponent of 2 is chosen to be a parabolic shape as in the PBL mixing. As a rule of thumb, $w = 1\ \mathrm{m\,s^{-1}}$ and $\delta = 60$ m over the tropical oceans when the turbulence mixing is maximized, giving us $K = 28\ \mathrm{m^2\,s^{-1}}$ at the cloud base ($z_b = 0$), for $RH = 0.8$, $D = 2$ km, and $h = 0.6$ km. Because of the parabolic profile in (4), K is decreased rapidly with height, and $K = 5\ \mathrm{m^2\,s^{-1}}$ in the middle of the cloud. The maximum and minimum of K are set as $50\ \mathrm{m^2\,s^{-1}}$ and $0.1\ \mathrm{m^2\,s^{-1}}$, respectively.

In the revised scheme, the height of cloud bottom and top is newly defined. Additional triggering conditions of a parcel in the sub-cloud layer are also designed. The cloud bottom is assumed to be the top of the PBL, rather than the LCL in the original TDK scheme. The height of LCL and h is very similar in well-mixed conditions, whereas LCL is higher than h, otherwise. For checking the buoyancy of a parcel originating at the maximum moist static energy level, the traveling depth between the parcel originating level and the cloud bottom is limited to 1 km. Also, another buoyancy checking of a parcel is the depth between the cloud bottom and the level of free convection, which is also limited to 1 km. The cloud top is defined as a lower level of the minimum moist static energy above the cloud bottom and a level of about 3 km from the

surface (sigma = 0.7). Convection is suppressed if the cloud appears at a single model level. Additional buoyancy checking of an updraft parcel in the proposed scheme plays a role in suppressing the activation of shallow convection. Also, note that parameters in the K-profile (4) are highly tunable toward a better skill of model prediction.

d. Experimental design

Six experiments were designed to permit investigation of the impact of the shallow convection on the simulated results. RA2_TDK experiment employs the physics package with the RA2 CPS scheme (Park and Hong, 2007), and Tiedtke SCV scheme (Tiedtke et al., 1988) for deep precipitation convection and shallow convection, respectively. RA2_NO experiment that excludes the TDK scheme from RA2_TDK experiment is conducted to confirm the role of shallow convection on the simulated climatology. RA2_modTDK replaces the TDK scheme with the modifications, which was described in section 2c. GFS_NO, GFS_TDK, and GFS_modTDK experiments replacing the CPS of Park and Hong (2007) with Han and Pan (2011) are to investigate the dependency of shallow convection on the deep convection algorithm. Note that the GFS CPS improves significantly the skill of weather forecasting over the RA2 GFS (Han and Pan, 2011). The five members of ensemble runs in each experiment are performed with initial data at 0000 UTC 1-5 May for boreal summer (June-July-August) of the years 1996, 1997, and 1999. These three years are regarded to be a normal, El Niño, and La Niña years, respectively, in terms of sea surface temperature in the eastern Pacific (Byun and Hong, 2004). These summers have been selected in investigating the simulated climatology in the GRIMs framework (Hong et al., 2013).

The means of the 15 simulations in each experiment are obtained and discussed. The observed precipitation and the observed large-scale fields are obtained from the Climate Prediction Center (CPC) Merged Analysis Monthly Precipitation (CMAP) data (Xie and Arkin, 1997) and the NCEP-Department of Energy (NCEP-DOE) Reanalysis II dataset (R-2; Kanamitsu et al., 2002b), respectively. The International Satellite Cloud Climatology Project (ISCCP) D2 data is used to compare the low-level cloudiness (Rossow and Schiffer, 1999; Iacobellis and Somerville, 2000). All the simulations were performed with the horizontal resolution corresponding to the spectral truncation of T62 (triangular truncation of wavenumbers at 62, corresponding roughly to about 200 km) and a 28-layer terrain-following sigma coordinate in vertical dimension. There are 10 layers below 850 hPa and the model top is about 3 hPa.

3. Results and discussion

a. Zonal mean temperature and moisture

It is apparent that the GRIMs model is able to reproduce the zonally averaged temperature and relative humidity from a climatological point of view, even in the absence of shallow convection scheme (Figs. 1a, b). Except for warm biases in the upper troposphere over the tropics and in the lower troposphere in mid-latitudes, it is obvious that cold biases are prevalent throughout the troposphere (Fig. 1a). In the lower troposphere, cold biases are distinct over the sub-tropics, in which axes of biases are inclined to high latitudes with height. For moisture, dryness is prevailing throughout the troposphere, except for wet bias at high latitudes in the middle- to upper troposphere (Fig. 1b). Dryness above 900 hPa is pronounced, with a maximum over the tropics. A layer with a distinct dry bias appears in the upper troposphere over the tropics and sub-tropics.

Figures 1c, d confirm a typical role of shallow convection by transporting moisture and heat above the boundary layer. For temperature, the cold bias below 900 hPa is reduced, as expected, but cooling in the mid-troposphere tends to worsen the bias (Fig. 1c). Moistening above the boundary layer reduces the significant dry bias centered over the tropics (Fig. 1d). Warming near the surface is also observed by the modified TDK SCV scheme, but with a greater magnitude than that in the original TDK scheme (cf. Figs. 1c, e). In contrast to the cooling effect above the boundary layer in the case of TDK SCV experiment, modTDK SCV experiment warms the troposphere up to 200-hPa level, which leads to the improvement of simulated climatology. The direct sequence of shallow convection should bring about cooling above the PBL top. Thus, the warming effect in modTDK run can be attributed to an indirect effect due to interaction with shallow convection and other processes. In Table 2, it is noted that the amount of convective precipitation is increased when the modTDK scheme is used, whereas the increase is not discernible in the case of the original TDK scheme. In particular, the convective rainfall is suppressed when the original TDK SCV scheme is introduced particularly over the Western Pacific Region, whereas its increase is prominent in the case of the modTDK SCV scheme. This finding indicates that the warming due to enhanced heating by the deep convection scheme overwhelms the cooling effect in the lower troposphere by the shallow convection scheme, when the modified SCV TDK scheme is employed. Meanwhile, moistening above the boundary layer appears as in the case of TDK run, but with a narrower width in latitudes when the modified TDK SCV scheme is employed (Fig. 1f). The tabulated scores in Table 1 generally manifest the overall improvement of the lower tropospheric structure but the skill of the simulated precipitation in Table 2 shows mixed effects by the modified scheme proposed in this study.

Figure 2 evaluates the role of the shallow convection processes in conjunction with the deep convection processes. It is clear that the thermodynamic structure is in better agreement with the R-2 data even in the absence of the shallow convection module (cf. Figs. 1ab, 2ab). The RMSE and bias scores in Table 1 confirm a better performance of the GFS CPS over the RA2 CPS. In particular, the dry bias in the upper troposphere

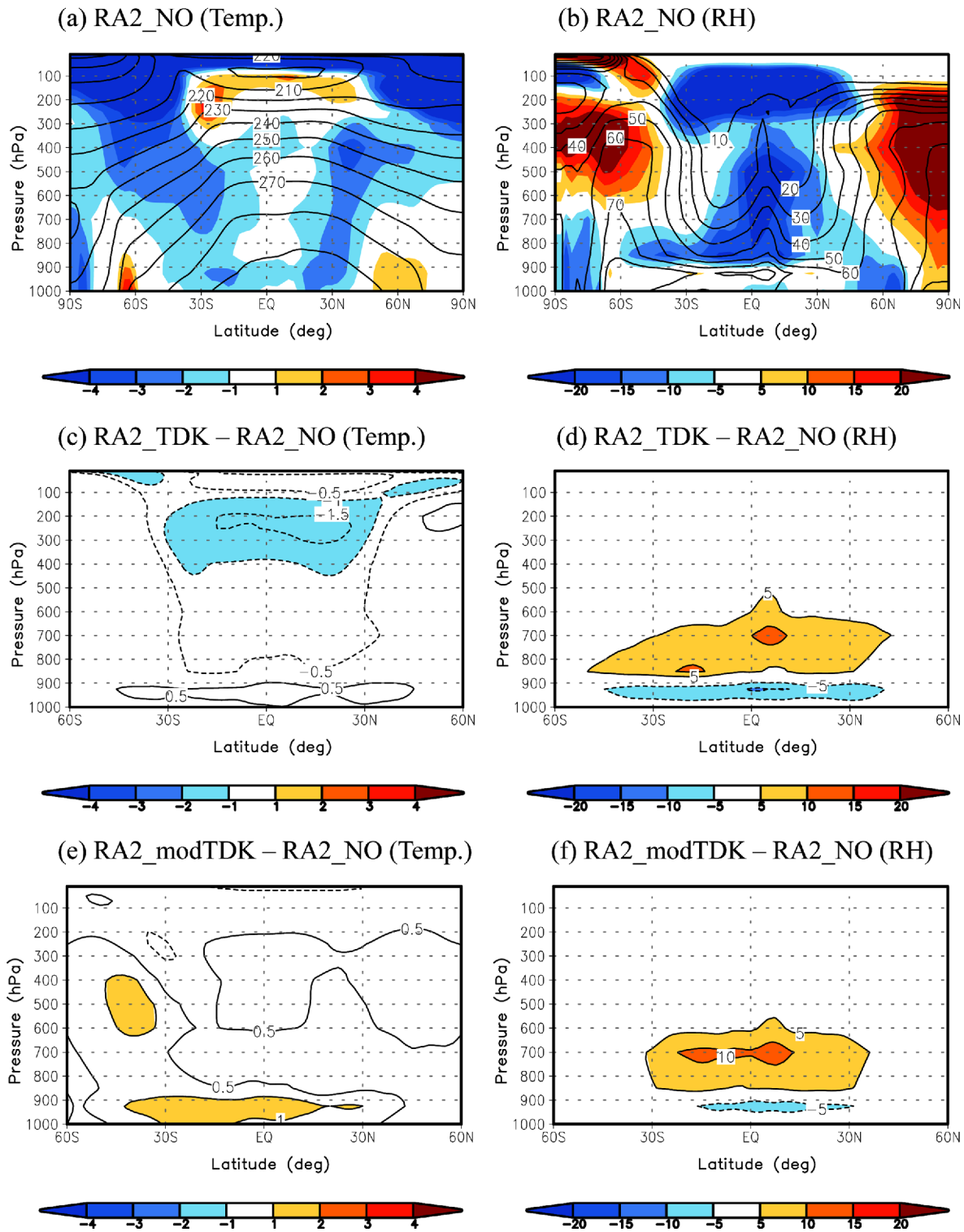

Fig. 1. Zonal mean averages for the three boreal summers (1996, 1997, and 1999) of (a) temperature (K) and (b) RH (%) obtained from RA2_NO experiment (contour) and the corresponding differences from the R2 data (shaded). Differences of RA2_TDK and RA2_modTDK from the RA2_NO simulation are shown in (c, d) and (e, f), respectively.

is remarkably reduced when the GFS CPS is used (cf. Figs. 1b, 2b), which is a direct effect of overshooting clouds, as designed by Han and Pan (2011). The original TDK SCV scheme shows mixing in a similar fashion for both RA2 and GFS CPS experiments, although the cooling effect in the upper troposphere is reduced when the GFS CPS is used (cf. Figs.

Table 1. Statistics of the bias and root mean square errors (RMSE) for three-summer averaged zonal-mean climatology of temperature (K) and relative humidity (%) below 700 hPa between the NCEP reanalysis data (RA2) and the simulations. Values in parentheses are averaged between 700 hPa and 100 hPa. The best score is highlighted as bold numbers.

Experiment	Temperature		Relative Humidity	
Name	Bias	RMSE	Bias	RMSE
RA2_NO	−1.03 (−1.56)	2.02 (2.89)	−7.12 (−7.57)	14.34 (20.29)
RA2_TDK	−1.08 (−2.07)	2.07 (3.01)	−5.32 (−5.93)	11.63 (19.32)
RA2_modTDK	−0.51 (−1.13)	1.73 (2.63)	−4.36 (−5.70)	11.76 (19.34)
GFS_NO	**−0.25** (−1.46)	1.57 (2.75)	−4.37 (3.24)	11.79 (**13.70**)
GFS_TDK	−0.28 (−1.90)	**1.48** (2.88)	−4.28 (**2.37**)	11.81 (14.91)
GFS_modTDK	0.32 (**−0.89**)	**1.48** (**2.62**)	**−2.91** (2.94)	**11.17** (15.13)

Table 2. The 3-year averaged global mean precipitation (mm day^{-1}), and the RMSE and the Pattern Correlation (PC) coefficients for the simulated precipitation (mm day^{-1}) compared with the CMAP observation. The values in brackets are the statistical values of averaged for the Western Pacific region (110°E-180°E, 20°S-30°N). The best score is highlighted as bold numbers.

Experiment	Amount (mm d^{-1})	RMSE	PC	Convective precip (mm d^{-1})
CMAP	2.70 (5.73)			
RA2_NO	3.33 (7.32)	2.58 (4.85)	0.71 (0.40)	2.85 (7.20)
RA2_TDK	3.26 (6.91)	2.40 (3.94)	0.74 (0.48)	2.85 (6.90)
RA2_modTDK	3.41 (7.42)	2.49 (3.67)	0.75 (0.65)	2.97 (7.40)
GFS_NO	2.96 (6.00)	2.05 (3.00)	**0.76** (0.61)	2.32 (5.68)
GFS_TDK	**2.93** (**5.71**)	**2.00** (**2.54**)	0.75 (0.67)	2.42 (5.65)
GFS_modTDK	3.09 (6.28)	2.13 (2.60)	**0.76** (**0.75**)	2.48 (6.15)

1c, 2c). The intensity of moistening within shallow clouds and drying below the cloud base is smaller (cf. Figs. 1d, 2d). Drying in the upper troposphere in the presence of the GFS CPS can be an indirect effect that is associated with parameterized deep convection processes. This point will be further addressed later.

In the case of the modified TDK SCV scheme with the GFS CPS (Figs. 2e, f), heating effect above the PBL top is enhanced, but moistening in the lower troposphere is suppressed, which indicates a overall weakening of shallow convection (cf. Figs. 1ef, 2ef). The enhanced heating in Fig. 2e reflects the increase of convective heating due to the deep convection scheme, as seen in Table 2. Since the GFS CPS already corrects the inherent biases, the role of the shallow convection scheme is limited in the case of the modTDK SCV scheme, whereas the original TDK scheme shows a similar magnitude of mixing, irrespective of the choice of CPSs.

b. Precipitation and cloudiness

In Fig. 3, the simulated precipitation climatology from 6 experiments is compared with the CMAP data. The overall distribution of tropical rainfall from all the experiments is acceptable as compared to the observed, but with an exaggerated ITCZ over the tropics and a deficit in the tropical maritime continent over the western equatorial Pacific, regardless of the physics package being used. It is noted that experiments with the GFS CPS alleviate the intense rainfall core along the ITCZ in the case of the RA2 CPS (cf., Figs. 3bc, 3ef). In particular, an excessive spurious precipitation northeast of Australia is significantly reduced when the GFS CPS is employed. The RMSE and pattern correlation coefficients in Table 2 confirm the overall improvement of the simulated precipitation by the GFS CPS, as compared to the RA2 CPS, irrespective the choice of SCV scheme. In the table, it can be seen that for both CPS experiments the original TDK scheme reduces the amount of precipitation when compared to the results in the absence of shallow convection, whereas it is increased when the modTDK SCV is used. modTDK SCV run degrades the skill of simulated precipitation in terms of its amount, but its pattern correlation is improved over the experiments with the original TDK scheme.

A close inspection of Fig. 3 reveals visible differences in precipitation over the equatorial western Pacific between the original and modified TDK experiments. Precipitation in Indonesia and adjacent oceans is increased in modTDK experiment toward what was observed when the RA2 CPS is used (Figs. 3c, d). The subtropical precipitation to the east of Philippines is also improved by the modified TDK SCV scheme when the GFS CPS is employed (cf. Figs. 3f, g), which results in the improvement of the pattern correlation (Table 2). From Table 2 and 3, it can be seen that a more organized precipitation over the western Pacific in the case of the modTDK scheme in Fig. 3 is associated with the enhanced

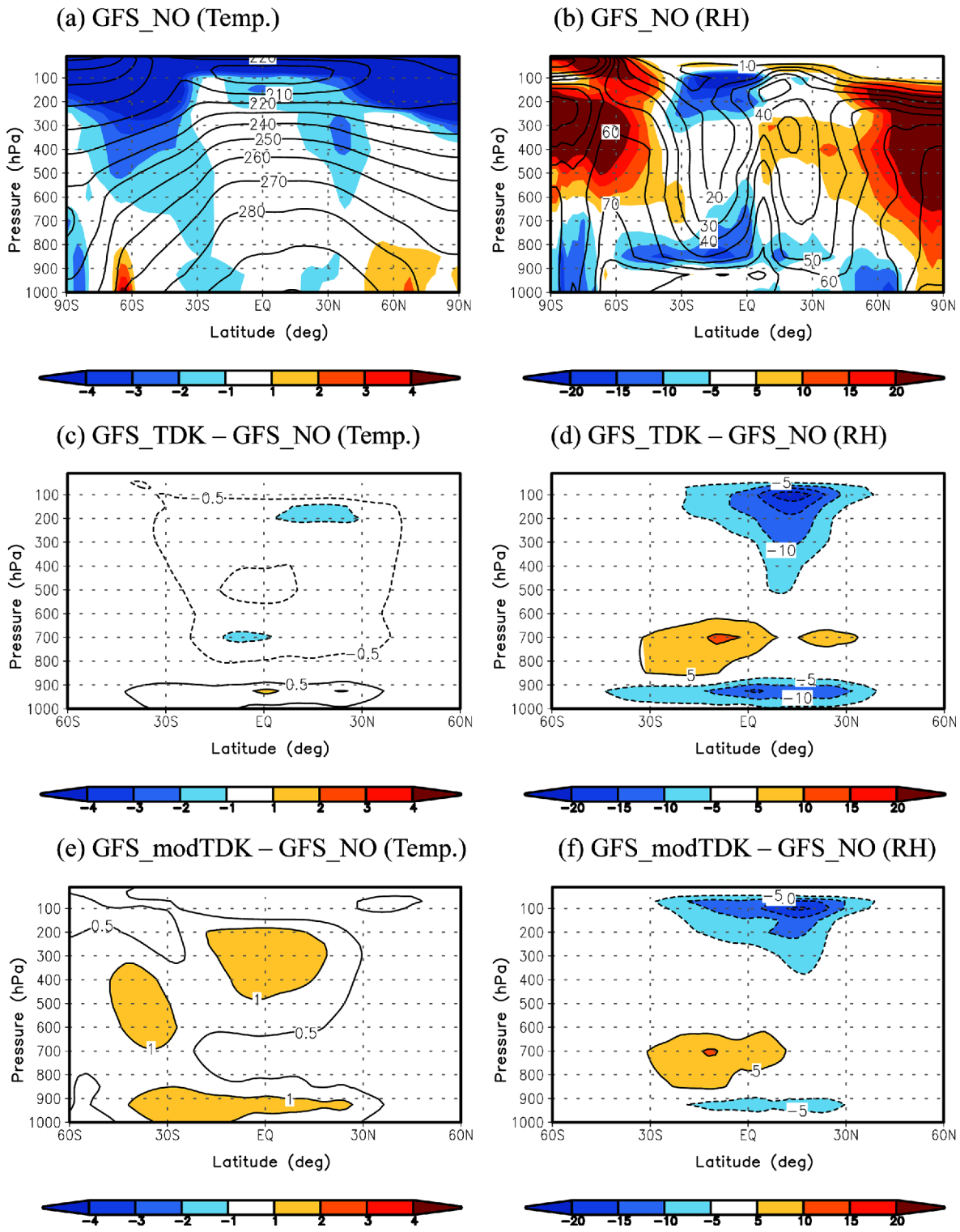

Fig. 2. Same as Fig. 1 but with the GFS CPS scheme.

precipitation due to the cumulus parameterization scheme, together with the enhanced low clouds, which indicates a less activation of shallow convection. Note that in the GRIMs the shallow convection is turned off when the cumulus parameterization scheme is activated.

Figure 4 compares the distribution of low-level cloudiness, which is a variable that is directly modulated by the shallow convection module, when non-precipitating maritime strato-

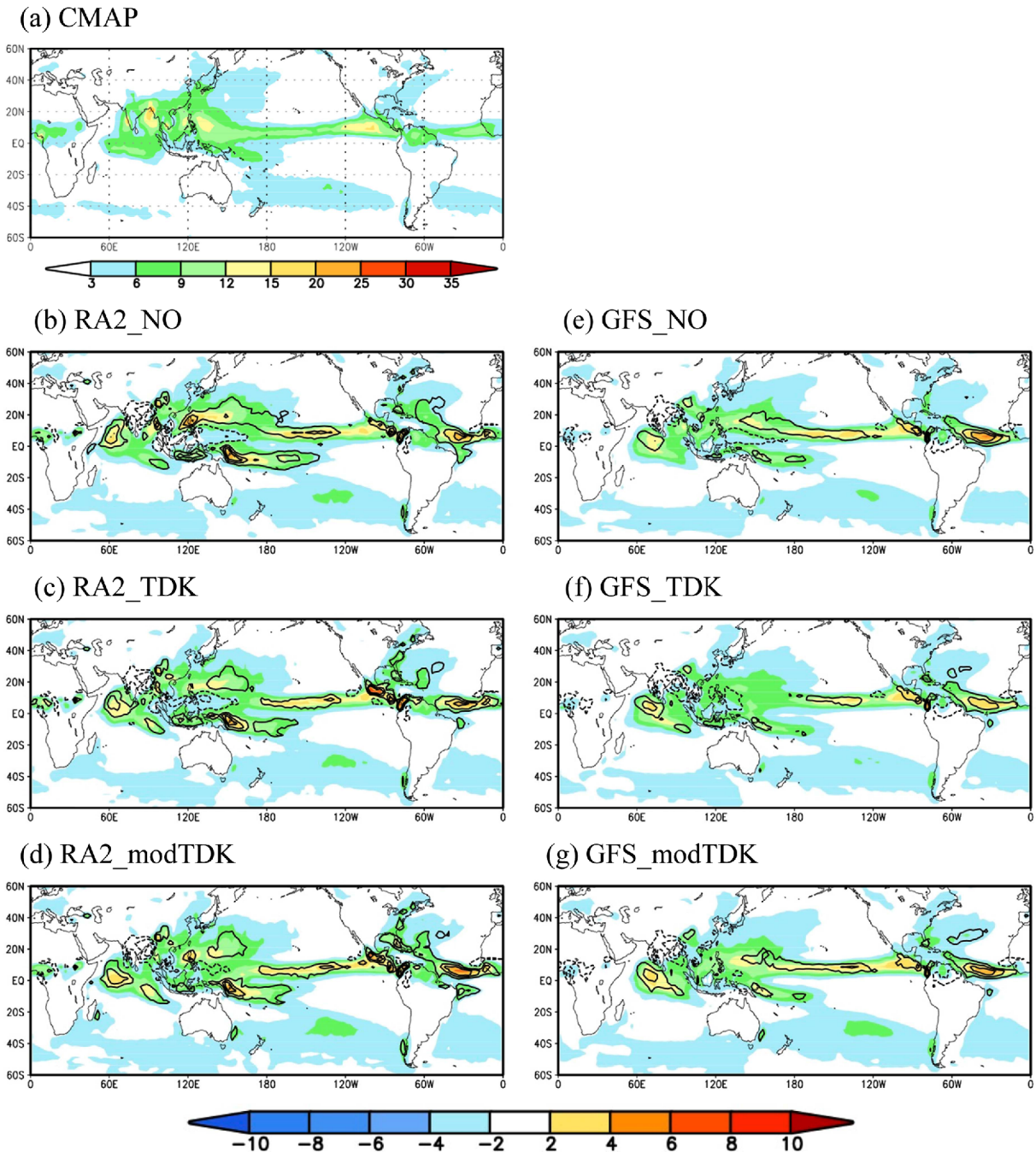

Fig. 3. (a) Distribution of 3-year averaged daily precipitation (mm day^{-1}) obtained from the CMAP observation. (b)-(g) Difference of the precipitation between each experiment and the CMAP observation. Solid and dashed contour lines (interval 4 mm day^{-1}) denote positive and negative biases, respectively.

cumulus clouds exist. It is noted that the modeled cloudiness is an average with the assumption of maximum overlapping between the surface and about 700 hPa level, whereas the observed cloudiness in Fig. 4a is a satellite estimate, which can underestimate the amount when deep precipitating convection exists, for example, over the ITCZ. For this reason, we will mainly focus on the subtropics where shallow stratocumulus clouds dominate, as done by Han and Pan (2011).

It is clearly seen that the low-level cloudiness over the tropics and mid-latitudes is mostly overestimated when the shallow convection is taken out, irrespective of the choice of CPS (Figs. 4b, e). The original TDK SCV scheme greatly reduces the amount of cloudiness over the global irrespective of CPS scheme (Figs. 4c, f). For example, clouds in eastern

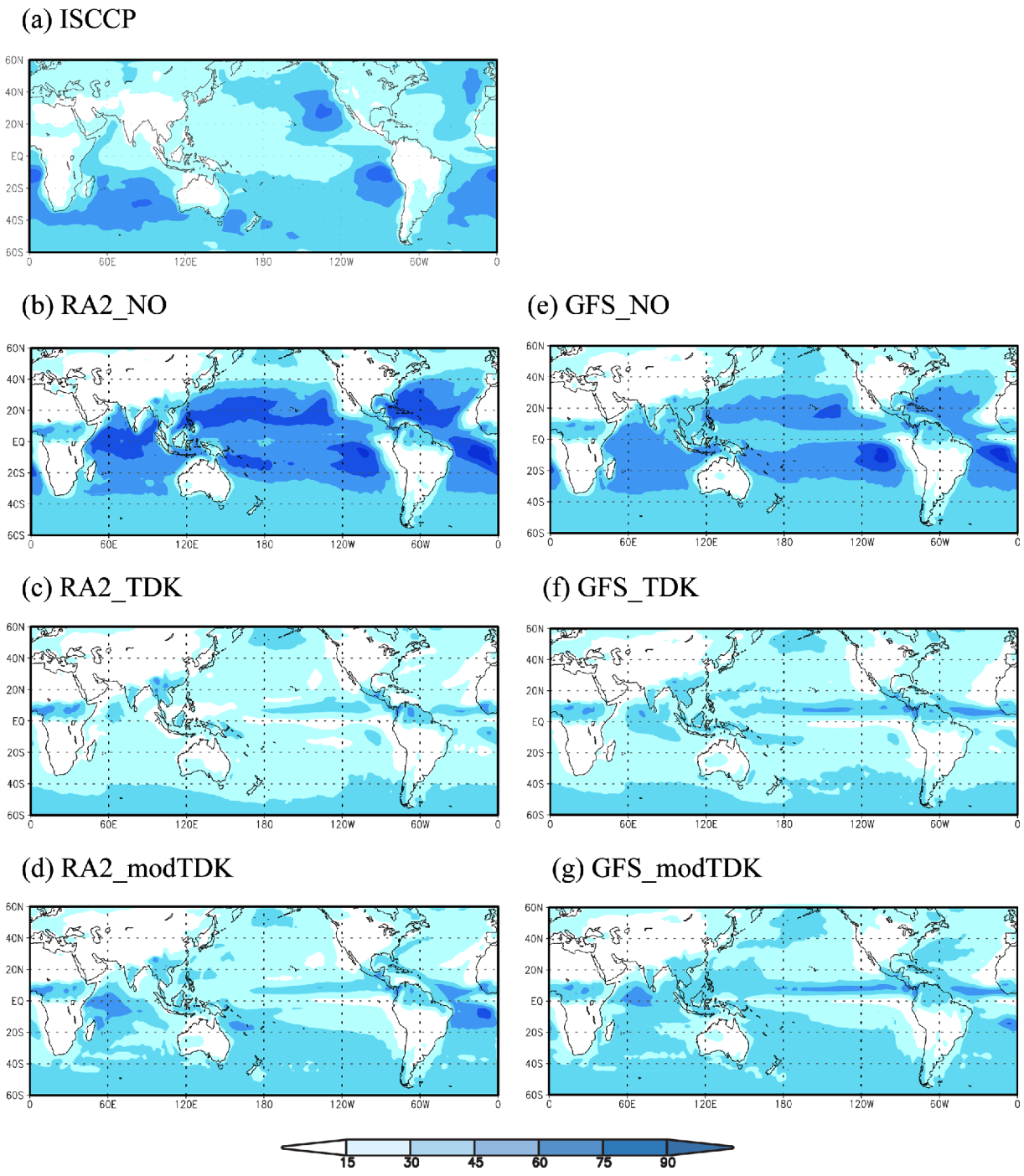

Fig. 4. Same as Fig. 3 except for the low-level cloudiness (%). Distribution of low-level cloudiness in (a) is from the ISCCP data.

Pacific, west of North America, and the southern hemispheric oceans are underestimated. This feature reflects too strong mixing by the original TDK scheme, as seen in Han and Pan (2011), resulting in the reduction of low clouds (Table 3). The modified TDK SCV scheme is able to improve the cloudiness in the southern hemisphere by increasing its amount for both CPS experiments (Figs. 4d, g). The negative bias in cloud cover in the eastern Pacific may be due to the relatively coarse horizontal resolution of approximately 200 km, together with the absence of ocean-coupled system (Li et al., 2012).

4. Concluding remarks

We have investigated the impacts of shallow convection scheme on a simulated seasonal climatology in a global atmospheric model. The eddy-diffusivity scheme of Tiedtke (TDK)

Table 3. The 3-year averaged global mean low-level cloud fraction (%), downward shortwave radiation flux at surface (W m^{-2}), boundary layer height (m) averaged for the tropics (20°S-20°N).

Experiment	Low cloud	Shortwave rad flux	PBL height
RA2_NO	43.3	220.0	790.3
RA2_TDK	20.0	249.4	671.6
RA2_modTDK	26.2	238.7	654.9
GFS_NO	38.3	212.9	668.5
GFS_TDK	24.2	234.0	534.2
GFS_modTDK	27.7	226.1	538.2

is evaluated, focusing on the dependency upon the deep convection schemes. Drying and warming near the top of the boundary layer and opposing effects above are observed. These effects are pronounced over the oceans, which leads to the modulation of tropical precipitation. It is also found that shallow convection suppresses the turbulent eddies within the PBL by warming the air near the PBL top (In Table 3, see lower PBL height when the shallow convection is turned on). The amount of low clouds decreases due to upward moisture transport (Table 3). Note that the averaged cloudiness for radiation transfer is estimated with the assumption of maximum overlapping of cloudiness in adjacent layers. In the table, it can be seen that the reduced low cloud enhances the downward short wave fluxes reaching the surface, which consequently modulates the sub-cloud properties. The weakened PBL turbulence is partly compensated by the increased downward solar radiation. It is found that the original TDK scheme shows similar effects regardless of the choice of the deep convection scheme. A revised TDK scheme that explicitly couples the planetary boundary layer and shallow convection is proposed and evaluated. Our results indicate that the original TDK scheme tends to exaggerate the mixing above the PBL top, which results in underestimation of low-level clouds. The proposed SCV scheme overall weakens the mixing, increasing the low level clouds. The proposed scheme generally improves the simulated climatology over the results with the original TDK scheme, along with further improvement in the case of the revised deep convection scheme.

In addition to different trigging conditions, the fundamental difference places in the shape of K-profiles between the original and modified schemes (Fig. 5). In the figure, it is obvious to see that the original TDK SCV shows nearly identical profiles, no matter which the region or deep convection scheme is employed (Figs. 5a, b). It is because the cloud base is close to the PBL top and its top reaches the maximum limit of about 700 hPa over the tropics. Note that tropical atmosphere over the oceans is conditionally unstable up to about 600 hPa. The only difference is the height of the cloud base, with a lowering of it in the case of the GFS CPS scheme. The parabolic shape is preserved for all modTDK experiments, but its magnitude differs (Figs. 5c, d). The magnitude is smaller in the GFS CPS

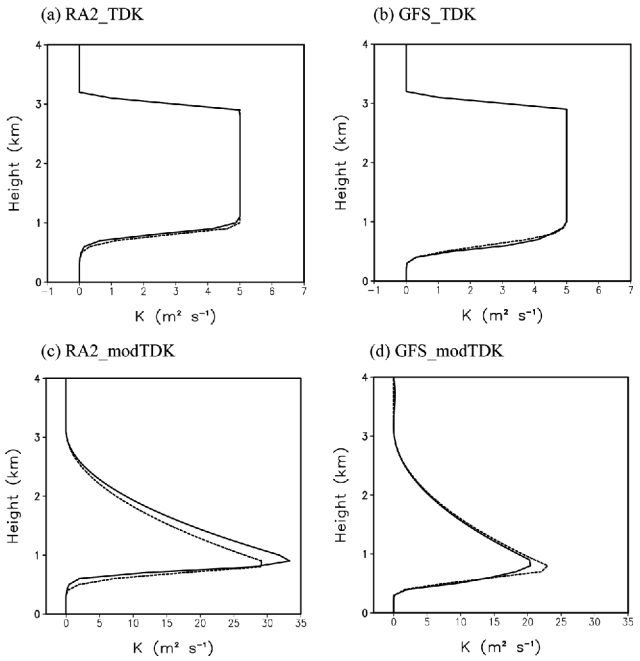

Fig. 5. Vertical profiles of eddy diffusivity (K, $m^2 s^{-1}$) from the (a) RA2_TDK, (b) GFS_TDK, (c) RA2_modTDK, and (d) GFS_modTDK experiments, averaged for the Western Pacific region (110°E-180°E, 20°S-20°N, solid) and for the Eastern Pacific region (90°W-180°W, 20°S-20°N, dashed). The profiles are constructed from the domain-averaged PBL and cloud properties as described in Section 2.

case than in the RA2 CPS, which confirms a weakening of shallow convection in the case of the GFS CPS. This indicates that the role of the shallow convection scheme is reduced when biases in the simulated climatology are largely corrected by deep convection processes due to the cumulus parameterization scheme. Restricted triggering considering the buoyancy of the updraft thermal, along with the parabolic shape K-profile that couples with the PBL properties, enables the deep convection to be activated vigorously (see Table 2). Realizing the fact that the GFS CPS is superior to the RA2 CPS, the behavior of the proposed shallow convection scheme over the western Pacific plays a positive role in improving the tropical precipitation core over the western Pacific (Fig. 3).

Out study further indicates that the simulated precipitation climatology is primarily modulated by the deep convection package, but the role of shallow convection module is not negligible. It is because the shallow convection modulates the sub-cloud properties directly when convective precipitation is activated. As in the interaction between the boundary layer processes and precipitation physics (e.g., Hong et al., 2006), understanding the interaction between the shallow convection and precipitation physics through the modulated boundary layer processes is important to enhance the skill of weather forecasting and climate simulation.

Acknowledgments. This work has been carried out through the

R&D project on the development of the global numerical weather prediction systems of the KIAPS funded by the Korea Meteorological Administration (KMA). The authors acknowledge Junhong Lee, Hyeyum Hailey Shin, Jimy Dudhia, and Wei Wang for implementing and evaluating the modified scheme in the weather research and forecasting (WRF) model (http://wrf-model.org).

Edited by: John Richard Gyakum

References

Betts, A. K., 1986: A new convective adjustment scheme. Part I: Observational and theoretical basis. *Quart. J. Roy. Meteor. Soc.*, **112**, 677-691.

Bogenschutz, P. A., A. Gettelman, H. Morrison, V. E. Larson, C. A. Craig, and D. P. Schanen, 2013: Higher-order turbulence closure and its impact on climate simulations in the Community Atmosphere Model. *J. Climate,* **26**, 9655-9676, doi:10.1175/JCLI-D-13-00075.1.

Bretherton, C. S., and S. Park, 2009: A new moist turbulence parameterization in the community atmosphere model. *J. Climate*, **22**, 3422-3448.

Byun, Y. H., and S.-Y. Hong, 2004: Impact of boundary-layer processes on simulated tropical rainfall. *J. Climate*, **17**, 4032-4044.

Gordon, C. T., A. Rosati, and R. Gudgel, 2000: Tropical sensitivity of a coupled model to specified ISCCP low clouds. *J. Climate*, **13**, 2239-2260.

Grell, G. A., 1993: Prognostic evaluation of assumptions used by cumulus parameterizations. *Mon. Wea. Rev.*, **121**, 764-787.

Han, J., and H.-L. Pan, 2011: Revision of convection and vertical diffusion schemes in the NCEP global forecast system. *Wea. Forecasting*, **26**, 520-533, doi:10.1175/WAF-D-10-05038.1.

Hartmann, D. L., M. E. Ockert-Bell, and M. L. Michelsen, 1992: The effect of cloud type on earth's energy balance: Global analysis. *J. Climate*, **5**, 1281-1304.

Hong, S.-Y., Y. Noh, and J. Dudhia, 2006: A new vertical diffusion package with an explicit treatment of entrainment processes. *Mon. Wea. Rev.*, **134**, 2318-2341.

_____, and Coauthors, 2013: The Global/Regional Integrated Model system (GRIMs). *Asia-Pac. J. Atmos. Sci.,* **49**, 219-243, doi:10.1007/s13143-013-0023-0.

Iacobellis, S. F., and R. C. J. Somerville, 2000: Implications of microphysics for cloud- radiation parameterizations: Lessons from TOGA COARE. *J. Atmos. Sci.*, **57**, 161- 183.

Jakob, C., and A. P. Siebesma, 2003: A new subcloud model for mass-flux convection schemes: Influence on triggering, updraft properties, and model climate. *Mon. Wea. Rev.*, **131**, 2765-2778.

Johnson, R. H., T. M. Rickenbach, S. A. Rutledge, P. E. Ciesielski, and W. H. Schubert, 1999: Trimodal characteristics of tropical convection. *J. Climate*, **12**, 2397-2418.

Juang, H.-M. H., and M. Kanamitsu, 1994: The NMC nested regional spectral model. *Mon. Wea. Rev.*, **122**, 3-26.

_____, S.-Y. Hong, and M. Kanamitsu, 1997: The NCEP regional spectral model: An update. *Bull. Amer. Meteor. Soc.*, **78**, 2125-2143.

Kanamitsu, M., and Coauthors, 2002a: NCEP dynamical seasonal forecast system 2000. *Bull. Amer. Meteor. Soc.*, **83**, 1019-1037.

_____, W. Ebisuzaki, J. Woollen, S.-K. Yang, J. J. Hnilo, M. Fiorino, and G. L. Potter, 2002b: NCEP-DOE AMIP-II Reanalysis (R-2). *Bull. Amer. Meteor. Soc.*, **83**, 1631-1643.

Klein, S. A., and D. L. Hartmann, 1993: The seasonal cycle of low stratiform clouds. *J. Climate*, **6**, 1587-1606.

Li, H., M. Kanamitsu, and S.-Y. Hong, 2012: California reanalysis downscaling at 10 km using an ocean-atmosphere coupled regional model system. *J. Geophys. Res*., **117**, D12118, doi:10.1029/2011JD-017372.

Ma, C.-C., C. R. Mechoso, A. W. Robertson, and A. Arakawa, 1996: Peruvian stratus clouds and the tropical pacific circulation: a coupled ocean-atmosphere GCM study. *J. Climate*, **9**, 1635-1645.

Norris, J. R., 1999: On trends and possible artifacts in global ocean cloud cover between 1952 and 1995. *J. Climate*, **12**, 1864-1870.

Pan, H.-L., and W.-S. Wu, 1995: Implementing a mass flux convective parameterization package for the NMC medium-range forecast model. NMC Office Note 409**,** 43 pp.

Park, H., and S.-Y. Hong, 2007: An evaluation of a mass-flux cumulus parameterization scheme in the KMA global forecast system. *J. Meteor. Soc. Japan*, **85**, 151-168.

Rossow, W. B., and R. A. Schiffer, 1999: Advances in understanding clouds from ISCCP. *Bull. Amer. Meteor. Soc.*, **80**, 2261-2287.

Stensrud, D. J., 2007: *Parameterization schemes: keys to understanding numerical weather prediction models.* Cambridge University Press, 459 pp.

Slingo, J., M. Blackburn, A. Betts, R. Brugge, K. Hodges, B. Hoskins, M. Miller, L. Steenman-Clark, and J. Thuburn, 1994: Mean climate and transience in the tropics of the UGAMP GCM: Sensitivity to convective parametrization. *Quart. J. Roy. Meteor. Soc.*, **120**, 881-922.

Tiedtke, M., W. A. Heckley, and J. Slingo, 1988: Tropical forecasting at ECMWF: The influence of physical parametrization on the mean structure of forecasts and analyses. *Quart. J. Roy. Meteor. Soc.*, **114**, 639-664.

Wu, C.-M., B. Stevens, and A. Arakawa, 2009: What Controls the Transition from Shallow to Deep Convection? *J. Atmos. Sci.*, **66**, 1793-1806.

Xie, P., and P. A. Arkin, 1997: Global Precipitation: A 17-year monthly analysis based on gauge observations, satellite estimates, and numerical model outputs. *Bull. Amer. Meteor. Soc.*, **78**, 2539-2558.

Zhang, Y., and S. A. Klein, 2010: Mechanisms affecting the transition from shallow to deep convection over land: Inferences from observations of the diurnal cycle collected at the ARM southern great plains site. *J. Atmos. Sci.*, **67**, 2943-2959, doi:10.1175/2010JAS3366.1.